Open Ceramics 2 (2020) 100010

Contents lists available at ScienceDirect

Open Ceramics

journal homepage: www.editorialmanager.com/oceram

Manufacturing of ceramic components with internal channels by a novel additive/subtractive hybridization process

Raphael de Melo Bernardino [a,b], Saverio Valentino [c], Giorgia Franchin [c], Jens Günster [a,b], Andrea Zocca [a,*]

[a] Division Ceramic Processing and Biomaterials, Bundesanstalt für Materialforschung und -prüfung (BAM), Unter Den Eichen 44-46, 12203, Berlin, Germany
[b] Institute of Nonmetallic Materials, Clausthal University of Technology, Zehntnerstr. 2a, Clausthal-Zellerfeld, 38678, Germany
[c] Department of Industrial Engineering, University of Padova, Via Marzolo 9, Padova, 35131, Italy

ARTICLE INFO

Keywords:
Additive manufacturing
Layerwise slurry deposition
Hybrid manufacturing

ABSTRACT

A new approach for fabrication of ceramic components with inner channels is proposed, as a result of the combination of two additive and one subtractive manufacturing processes. In this project, porcelain parts are manufactured by the Layerwise Slurry Deposition (LSD) process, meanwhile end milling and Direct Ink Writing (DIW) are applied to create channels on the surface of the deposited ceramic. Unique to the LSD process is the formation of a freestanding powder bed with a mechanical strength comparable to conventional slip casted ceramic green bodies. Combining these three processes allows the manufacturing of ceramic objects containing an internal path of ink, which in this case was a graphite-based ink that can be further eliminated by heat treatment to obtain a porcelain object embedded with channels. The results show the capabilities of this method and its potential to fabricate not only parts with inner channels, but also multi-material and multi-functional components (such as integrated electronic circuits).

1. Introduction

As Additive Manufacturing (AM) processes are technologically improving and a wider palette of materials is becoming commercially available, the frontier of research in this field is moving towards an increase of complexity of both equipment and products. This includes the development of processes for highly complex multifunctional [1–3], and multi-material objects [4–6]. In order to face some of these challenges, different types of hybrid AM technologies have been proposed for different applications. Following the definition by Sealy et al. [7] "hybrid AM processes are defined as the use of AM with one or more secondary processes or energy sources that are fully coupled and synergistically affect part quality, functionality, and/or process performance."

Hybrid AM technologies can be divided in two classes. (i) The first class includes the hybridization between AM and other (non-additive) processing technologies. Often this involves the hybridization of additive and subtractive (machining) manufacturing in the same platform. Especially when coupled to AM technologies with high material deposition rates, such hybrid processes can also achieve high productivity [8,9]. This approach is advantageous to retain the geometrical freedom offered by AM and at the same time improving the control over the geometrical tolerances and surface quality offered by machining [10]. The hybridization of powder bed fusion AM has also been proposed to improve the control of the microstructure or to reduce the thermal stresses, for example by hybridization with laser peening, shot peening or grain refinement by rolling [7]. (ii) The second class of hybrid AM includes the hybridization between two different AM technologies. This approach is particularly interesting when it enables the integration of multiple functionalities and multiple materials in a single process. Although the possible combinations of AM processes are countless, often the hybridization is between an AM technology used to manufacture the bulk of a component (such as powder bed fusion, vat photopolymerization, binder jetting etc.) and a second AM technology (such as direct ink writing or aerosol jetting) used for the deposition of a second phase (e.g. a silver paste) which adds a functionality to the component [11–13]. It is worth noting that, according to the definition of hybrid AM used here, the application of technologies in subsequent processes is not considered as "hybrid AM" in this context. An example of the latter case could be the manufacturing of a polymeric component by fused deposition modelling followed by writing of conductive tracks by aerosol deposition [14], since

* Corresponding author.
E-mail address: andrea.zocca@bam.de (A. Zocca).

https://doi.org/10.1016/j.oceram.2020.100010
Received 5 April 2020; Received in revised form 26 May 2020; Accepted 28 June 2020
Available online 2 July 2020

the two processes are not "fully coupled".

The current work presents a hybrid AM process which is based on the Layerwise Slurry Deposition (LSD) technology. In the LSD process, a doctor blade is used to deposit a thin layer of a ceramic slurry over a heated porous platform which, by effect of capillarity and heat, forms a layer of dry ceramic powder. The deposition process is repeated in order to build several layers of highly packed ceramic powder on top of each other. A typical layer thickness in this process is between 100 μm and 200 μm [15,16]. Through combinations with other techniques such as laser sintering or binder jetting, it is possible to inscribe the cross-section of an object in each layer, thus producing a part layer-by-layer such as in typical powder bed additive manufacturing processes. The major advantage of the LSD process over other AM powder bed processes is that it generates a freestanding powder bed with a mechanical strength comparable to conventional slip casted ceramic green bodies and, thus, with high green density, making possible to obtain dense ceramic products after heat treatment.

The approach proposed in this work, named "hybrid LSD-DIW" consists in the hybridization of (i) the LSD deposition of ceramic powder layers, (ii) the machining of a path in the deposited ceramic layers and (iii) the deposition of an ink (ceramic, metallic or polymeric) by direct ink writing (DIW) to fill the machined volume. These three processes are fully integrated and thus respect the definition of hybrid AM according to Sealy et al. This hybrid process enables the AM of a ceramic material containing a complex structure of one or multiple secondary phases.

An interesting combination of two material phases in the hybrid LSD-DIW is the use of a sacrificial ink to integrate complex channels in a ceramic substrate. Complex channels in ceramic components are an essential feature for many applications ranging from ceramic heat exchangers [17] to chemical micro-reactors [18,19]. Although complex channels can be produced in most AM processes, in many cases (especially in powder bed fusion, binder jetting and vat photopolymerization) the untreated material must be removed to free the channel, which can be very challenging for fine and complex geometries.

The hybrid LSD-DIW approach synergistically (i) enables the shaping of channels with complex geometries by machining, while at the same time (ii) ensures that the channels are not obstructed. The latter is achieved by filling them with a sacrificial ink, which is removed in a subsequent heat treatment.

This manuscript describes for the first time the hybrid LSD-DIW process, combining the layer-by-layer deposition of a freestanding flat ceramic body with the machining of complex channels filled by DIW with a sacrificial graphite ink. Future perspectives to utilize this hybrid technology to produce multi-material complex-shaped 3D parts are discussed in the Outlook section.

2. Materials and methods

2.1. LSD-DIW hybrid process

The LSD-DIW hybridization process is the combination of two additive and one subtractive manufacturing technologies, where each one has an essential function to produce multi-material parts or ceramic parts with complex internal structures. The process here proposed uses the Layerwise Slurry Deposition (LSD) as the process of choice to deposit ceramic layers, whereas machining is used to remove portions of the layer and DIW is used to fill the machined volume in between those layers.

An overview of the process is shown in Fig. 1, depicting the three steps of the process that are repeated. In detail, the three steps are: (i) a predetermined number of ceramic layers is deposited by the LSD technology. Each layer is individually dried, forming a highly compact freestanding powder bed. Depending on the desired depth of machining, only one or multiple layers can be deposited at this stage; (ii) machining (end milling) is employed to remove material over the surface of the ceramic layers; (iii) the volume of material which was removed by machining is filled with an ink of a second phase. The method of choice to deposit the sacrificial ink was DIW using a screw displacement extruder, which offers a good control in dosing the ink. The three steps are repeated until the part is completed. The final product is a block of ceramic green body with an inner channel filled with ink. The shape of the block is defined by the shape of the base plate.

In the current study, the focus was on demonstrating the production of empty channels, thus the filler material of choice was a sacrificial graphite ink. For different applications, the filler material could be a second ceramic phase or a metal phase, such as an electrically conductive ink. Porcelain was used as a model ceramic material to demonstrate the feasibility of the process.

The equipment used in this project consisted of a combination of a robot arm (RV-E4NM, Mitsubishi, Japan), which was used both for the machining and for the ink deposition processes, assembled in a LSD custom machine. The robot has a positioning repeatability of 30 μm, according to the manufacturer's specifications. For the machining process, a rotating multi-tool (Dremel 4000, Dremel, Germany) with a flex shaft attachment (Dremel flexible shaft 225, Dremel, Germany) was attached to the robot arm. A 0.9 mm diameter drill bit (CEREC, Sirona Dental Systems GmbH, Germany) was used as tool to machine the channel. Also attached to the robot, orthogonal to the milling tool, was the extrusion head (Vipro-HEAD3, ViscoTec, Germany) with a stainless steel tip (Nordson EFD, USA). The extrusion head has a displacement volume of 0.03 mL/revolution, corresponding to a minimum extrusion rate of 0.3 mL/min.

In this work, a tip with 0.84 mm in inner diameter was used for the deposition of the sacrificial ink.

The LSD process was performed with a layer thickness of 150 μm on a square porous platform of size 20 × 20 cm^2. The slurry was poured in a reservoir enclosed between two parallel blades (with a 10 mm gap between the blades) mounted on an axis moving along the length of the platform. The distance between the platform and the reservoir was used to define the thickness of the layers during the slurry deposition. The porous platform used as substrate was heated to 120 °C to assist the elimination of water after the deposition of slurry, with a drying time of 30 s between layers. For the machining of a channel with 0.9 mm designed depth, a typical process was run with a speed of the milling tool set at 8 mm/s and a rotation of the tool at 8000 rpm. The extruder speed for the ink deposition was set at 10 mm/s. After hybrid manufacturing

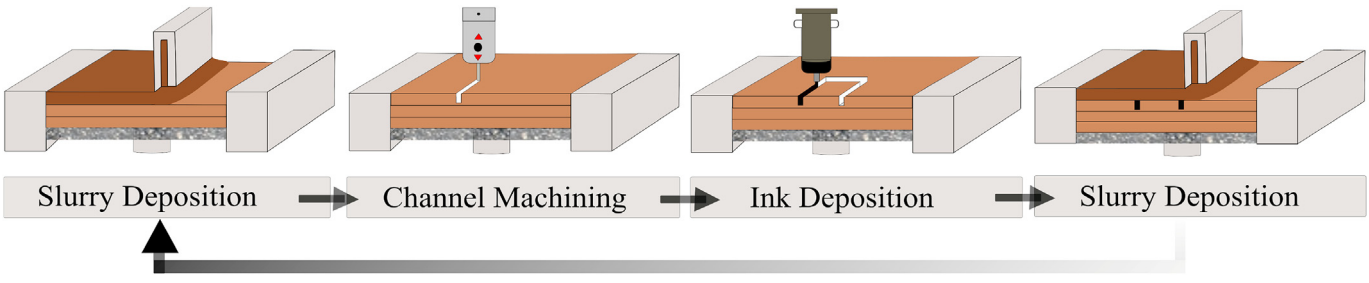

Fig. 1. Process schematic of the hybrid LSD-DIW.

and drying, the produced parts were subjected to heat treatment to remove the ink and to densify the ceramic material.

2.2. Raw materials

The porcelain slurry (Villeroy and Boch, Germany) used in the process was characterized by its particle size distribution by laser diffraction in water (Mastersizer 2000, Malvern, UK). The phase composition of the porcelain was determined by X-ray diffraction (D8 Advanced, Bruker AXS, USA) on a dried slurry.

Graphite ink was used as sacrificial material. The ink formulation contained 41 % wt of crystalline graphite powder 325 mesh (Alfa Aesar – Johnson Matthey Company, USA) in poly-propylene glycol 2000 (Sigma-Aldrich, USA). The particle size of the graphite powder was characterized by laser diffraction in air (Mastersizer 3000, Malvern, UK).

2.3. Thermal treatments

The sintering behavior of the porcelain was investigated by hot stage microscopy (Hesse-Instruments, Germany). For the HSM measurements, the powder was pressed to a cylindrical shape with 3 mm in diameter and in height. The pressed sample was placed on an α-alumina substrate and placed in the small oven of the instrument. A camera recorded images of the outline of the sample and the variation in the section area and shape of the sample was analyzed by software during heating up to 1500 °C with a heating rate of 10 °C/min.

A thermogravimetric and differential scanning calorimetry analysis (Mettler Toledo TGA/DSC 3+ STAR^e System, USA) was performed on the ink to determine a proper thermal treatment for the elimination of the ink. The analysis showed a total elimination of the graphite at 700 °C.

Based on the results of these studies, an optimized heat treatment of the parts produced by hybrid LSD-DIW process was defined: the burnout of the ink was performed by heating the parts in air with a heating rate of 10 °C/min up to 700 °C and 60 min dwelling time. This was followed by sintering of the ceramic at 1300 °C for 1 h with heating rate of 10 °C/min and a cooling rate of 5 °C/min.

2.4. Rheological characterization of the feedstocks

The rheological behavior of both the slurry and the ink was characterized in a rotational rheometer (MCR 301, Anton Paar GmbH, Germany). The flow curves were measured under controlled shear rate using a 25 mm diameter plate-plate system, in a range from 10 to 1000 s^{-1} for the slurry and 0.01 to 150 s^{-1} for the ink. The graphite ink was also tested in a strain sweep test using a 50 mm diameter cone-plate system, with a logarithmic strain ramp from 0.001% to 100% at 1 Hz frequency.

Additionally, an evaluation of the flow rate and the thickness of the extruded ink was performed directly in the LSD-DIW setup machine. The ink flow rate was correlated to the extruder rotation speed by measuring the weight (using a laboratory balance with an accuracy of 0.01 g) of extruded ink in a time of 60 s. The mass flow rate was converted to a volume flow rate assuming a density value of 1.25 g/cm^3 for the ink, calculated from the theoretical density of the single components using the rule of mixtures.

Using the extruder mounted on the robot arm, single lines of ink were deposited on a porcelain layer, keeping constant the linear velocity (10 mm/s) and the distance between extruder tip and layer (0.75 mm). The width of the lines was measured with a digital microscope (VHX digital microscope, Keyence, Germany) in dependence of the ink flow rate in the range 3–13 mm^3/s.

2.5. Characterization of the channel geometry

The continuity of the channels filled with ink in the ceramic green body was evaluated by testing the electrical conductivity of the ink traces. In fact, the ink is mainly composed of graphite and after drying it has a sufficient packing density to reach the percolation rate at which the extruded filaments are electrically conductive. Assessment of the channel geometry after burnout of the ink was carried out by visually inspecting the cross-section of the sample under an optical microscope (VHX digital microscope, Keyence, Germany). Computed X-ray tomography (μCT 40, Scanco Medical, Switzerland) was additionally performed on selected components after sintering. Proof of functionality of the channel after sintering was performed by injecting a liquid into one of the extremities and verifying the flow of the liquid on the other extremity of the channel.

3. Results and discussions

3.1. Raw materials

Table 1 summarizes the characteristics of the slurry and of the ink used in this project. The XRD results for the slurry showed an increase in mullite and cristobalite phases after sintering. The particle size of the porcelain was compatible with the layer thickness used (150 μm). For the graphite powder, the measured D(v, 0.9) was slightly larger than the specification of the manufacturer (i.e. 350 mesh), but it was still suitable for the DIW process with a needle tip of diameter 0.84 mm. The sintering temperature reported in Table 1 was derived from the shrinkage and aspect ratio curves measured by hot stage microscopy. For the ink, the decomposition temperature was derived from the thermogravimetric analysis of a similar ink composition. Both results are provided in the Supplementary Information material.

3.2. Rheological behavior of the feedstocks

The slurry used for the LSD process should present a suitable rheological behavior to reliably deposit layers during the movement of the doctor blade. If a slurry has too high viscosity, it is possible that the deposition will be affected by a lack of material and incomplete spreading. On the other hand, if the slurry has a too low viscosity, it can leak from the doctor blade.

Fig. 2a shows a flow curve for the porcelain slurry in a range of shear rate from 10 to 1000 s^{-1}. The results indicated a small yield stress and a decrease of the viscosity at increasing shear rate until 100 s^{-1}. The behavior can be better interpreted by interpolation with the Herschel-Bulkley model, which resulted in a best fit for $\tau_0 = 0.80 \pm 0.08$ Pa, flow index of $n = 0.983 \pm 0.001$ and consistency factor $k = 0.544 \pm 0.005$. τ_0 corresponds to the yield stress determined from the flow curve and the flow index n is slightly below 1, indicating a shear thinning behavior [20]. During the layer deposition a typical shear rate is in the range 200 s^{-1} – 400 s^{-1}, corresponding to a measured viscosity of 1–2 Pa s, which from previous experience is well suitable for the process [21].

Fig. 2b shows a flow curve of the graphite ink under increasing shear rate. The curve shows that the graphite ink had a clear shear thinning behavior, but with did not show an evident yield stress. Fig. 2c shows the results of an oscillatory sweep test at increasing shear stress. The graphic shows a plateau region at low shear stress, in which the storage modulus (G′) is higher than the loss modulus (G″). The cross-over point at which G′

Table 1
Material characterization of the porcelain slurry and of the graphite ink.

		Porcelain Slurry	Graphite Ink
Composition	**Before sintering**	Quartz (50.4 wt%) Mullite (19.9 wt%) Kaolinite (17.2 wt%) Albite (12.6 wt%)	Graphite (41 wt%) PPG (59 wt%)
	After sintering	Quartz (29.5 wt%) Mullite (48.0 wt%) Albite (22.6 wt%)	N.A.
Particle Size		D(v,0.1) = 2 μm D(v,0.5) = 14 μm D(v,0.9) = 126 μm	D(v,0.1) = 7 μm D(v,0.5) = 27 μm D(v,0.9) = 61 μm

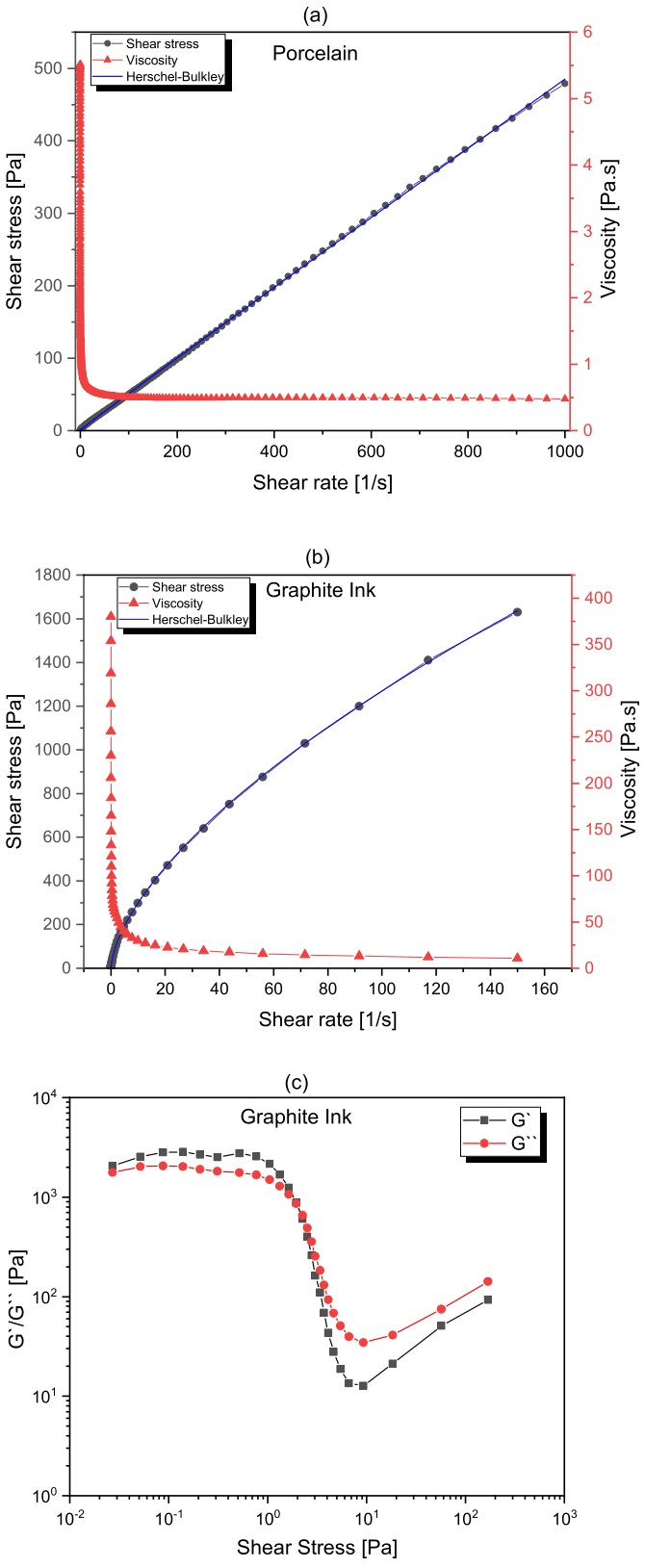

Fig. 2. Rheological characterization of the feedstocks (a) flow curve and viscosity curve of the porcelain slurry with interpolation by the Herschel-Bulkley model; (b) flow curve and viscosity curve of the graphite ink with interpolation by the Herschel-Bulkley model; (c) plot of the shear moduli of the graphite ink as a function of the oscillation stress at 1 Hz.

and G″ are equal corresponds to approximately 2 Pa. At higher shear stresses than the cross-over point, the loss modulus G″ is higher than the G' modulus, indicating a prevalently viscous behavior of the ink. The transition is not abrupt and can be understood as a moderate collapse of the microstructural organization of the material.

The viscosity of the ink at the shear rate relevant for the extrusion process (ca. 100 s^{-1}) was in the order of 10 Pa s, which is comparable to other published works [22–24]. The plateau values of G′ was approximately $3{\cdot}10^3$ Pa, while noticeably inks for DIW typically have much higher G′ values in the order of 10^4–10^5 Pa. A similar observation can be made for the cross-over point between G′ and G″, which is at very low stress in the graphite ink (2 Pa), consistently with the close to zero value of τ_0 determined from the flow curve. In comparison, typical DIW inks have a cross-over at up to 200 Pa [24]. The graphite ink in this work, in summary, can be described as a weak gel with low stiffness in the quiescent state.

According to the interpolation by Herschel-Bulkley model showed in Fig. 2b, the ink exhibited nearly zero yield stress ($\tau_0 = 0 \pm 1.08$ Pa) with a flow index $n = 0.62$ and a consistency factor $k = 70.68 \pm 0.75$. The flow index $n < 1$ indicates a more pronounced shear thinning behavior of the ink compared to the porcelain slurry. This behavior is beneficial for the DIW process, since it allows the ink to be extruded through fine nozzles.

It is important to notice here, that for Direct Ink Writing the ink must not only easily flow through the nozzle, but should also restore a high value of stiffness after deposition, so that it can sustain the forces applied by the successive layers of material deposited [22]. In the case of the hybrid LSD-DIW process, the requirements for the ink are however substantially different. The ink should indeed still easily flow through the nozzle, but once it is extruded it should homogeneously fill the channel machined in the ceramic layers. Since the filament is deposited in the channel with support from the bottom layer and from the sides of the channel itself, it is not necessary, and it can even be detrimental to use an ink with high stiffness. Once the channel has been filled, a gel-like behavior with G' > G″ at rest is favorable to avoid that the slurry deposited in the next ceramic layer displaces too much the graphite filling of the channel.

3.3. Machining and filling of the channels

Fig. 3 presents the stages of the process related to the machining of the channel and filling with ink. In Fig. 3a it is possible to see the channel after machining at the surface of the ceramic layer.

An important feature of the Layerwise Slurry Deposition is that the ceramic layers deposited by this technology have a high powder packing density, which is comparable to pressed or slip casted green bodies [21]. Consequently, the layers can be machined comparably to traditionally shaped ceramic green bodies. Nevertheless, the machining process is a delicate step, and should be performed with controlled material removal rate without generating a rough surface inside the channel. To achieve this, it is possible to remove material in steps where the robot repeats the same path, but with increasing depth. For the channels here presented, the total depth was 0.9 mm, which was achieved with three machining steps of 0.3 mm each.

Fig. 3b shows the channel filled with ink. The extrusion process started outside the channel, from the bottom side of the figure and following the spiral until reaching the end point in the middle. A small amount of ink was extruded outside of the part to ensure a stable flow inside of the channel. The amount of excess material at the beginning and end of the channel could be reduced by optimizing the synchronization between the control of the robot movement and of the extruder.

Lastly, Fig. 3c shows the finished part, which was completed by depositing six porcelain layers on top (0.9 mm total thickness) and by drilling a hole to connect the channel to the surface of the part.

In order to optimize the filling of the machined areas with ink, the extrusion width has to be controlled by tailoring the flow rate of the ink, which depends on the extruder geometry and can be controlled by

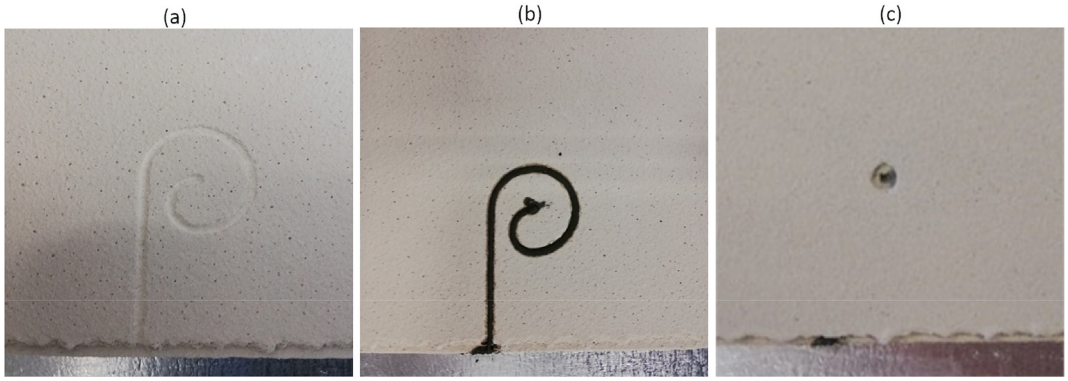

Fig. 3. Photographs of different stages of manufacturing of a channel: (a) after machining of the porcelain layers; (b) after filling with graphite ink; (c) after recoating and drilling from the top to connect the channel.

varying the speed of rotation. The velocity of movement of the extrusion head over the channel in this work was set to 10 mm/s, which provided a reliable performance of the robot unit used, with homogeneous deposition of material even in sharp corners.

Fig. 4a reports the ink flow rate from the extruder measured as a function of rotation speed, indicating a good linear correlation between the set extruder speed (in rpm) and the measured flow rate (in mm^3/s). From the flow rate, the maximum shear rate to which the ink is subjected can be calculated by:

$$\gamma' = 4Q/(\pi r^3)$$

Where Q is the volumetric flow rate and r is the nozzle radius. It was estimated that the shear rate was in the range between 90 s^{-1} to 106 s^{-1} depending on the extrusion parameters used (i.e. rpm). From these values, a value of viscosity of about 10 Pa s can be estimated from the measurements in Fig. 2b. It is relevant to notice that the shear rates are approximations estimated assuming a Newtonian behavior of the fluid.

The deposited ink width measured as function of the flow rate is shown in Fig. 4b. During the extrusion of the ink, the flow rate needs to be sufficient to continuously deposit material inside the channel. However, if the line deposited is too wide, this can cause an overflow at the edges of the channel or even outside, generating inhomogeneity of the channel and defects inside the ceramic material.

With the robot velocity and distance between the extruder tip and the channel base kept constants (10 mm/s and 750 μm respectively), the width of the deposited filament depends only on the extruder rotation speed. The measurements reported in the Fig. 4b show as expected a good linear correlation between flow rate and ink width.

The geometry of the channel at the end of the process, after burnout of the ink, depends both on the machined profile and on the flow rate of the ink. When the flow rate is enough to fill the whole machined volume, the final shape of the channel will be related to the shape created by the machining step, thus it will be square-like shape. In the case that the flow rate is not sufficient to completely fill the machined volume, the ink deposited will have a semi-circular cross-section as a result of the shape of the tip and the rheological behavior of the ink. The shape of the deposited ink remains mostly unaltered by the successive deposition of porcelain slurry, since according to Fig. 2c the ink is in a gel-like state (G' > G″) in the quiescent state. Therefore, the final shape of the channel will be round-like.

The channel profile after removal of the graphite ink (thermal treatment at 700 °C for 1 h) is shown in Fig. 5. The shape of this channel is related to a process with a low flow rate, approximately 5 mm^3/s, which resulted in a depth 0.73 mm (slightly less of the drilled depth of the channel), and it has a round-like profile. The image shows that the bottom of the channel has a flat shape, caused by the flat shape of the drill tool, but due to the rheology of the ink, the circular shape at the top is retained.

Two regions stand out in Fig. 5. Due to the empty space between the deposited ink and the walls of the channel, the new slurry deposited in the layers on top of the channel can partially fill the machined volume not already filled by the ink. In Fig. 5, the channel profile is perpendicular to the movement of the doctor blade, as indicated by the black arrow in the image.

As the porcelain slurry approached the deposited ink, it could clearly

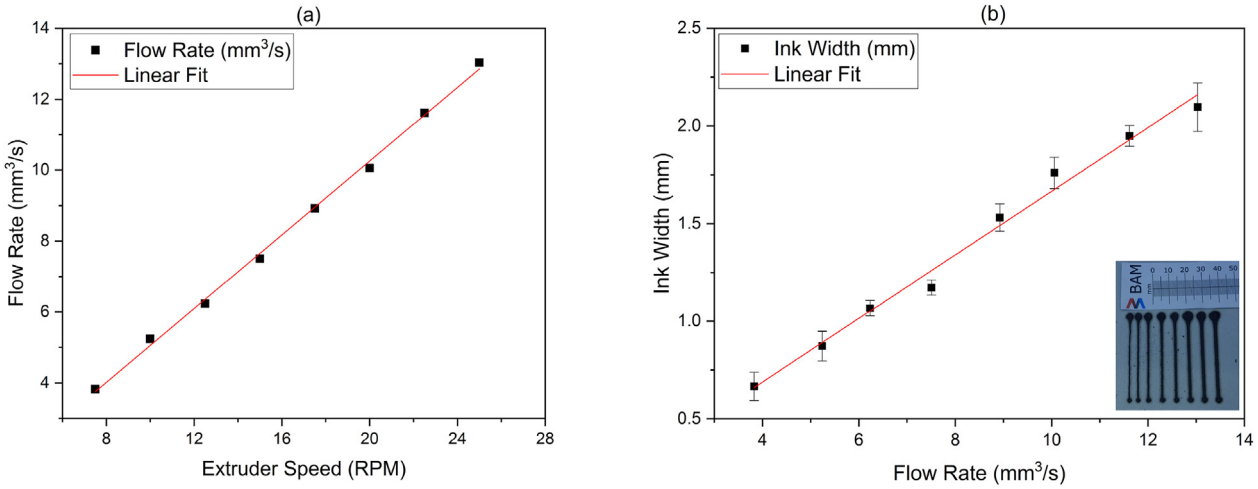

Fig. 4. (a) Flow rate from the extruder measured as a function of rotation speed and (b) width of lines extruded on a porcelain substrate as a function of the flow rate.

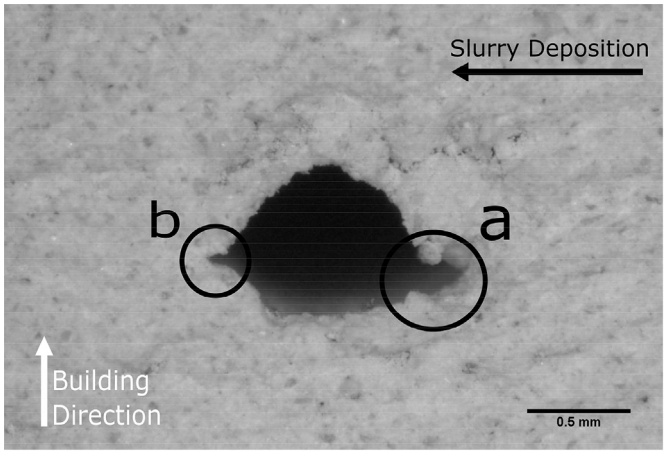

Fig. 5. Profile view of channel after burnout of the ink, highlighting (a) a large air pocket and (b) a smaller defect due to ink squeezing upon slurry deposition at the top.

not completely fill the empty space between the ink and the machined wall, leaving a large pocket of air. As the slurry deposition proceeded on top of the ink, it seems likely that it squeezed the ink to the side, forming a smaller defect after burnout of the graphite.

A major issue with these defects is that they may act as initiation for the formation of cracks during sintering. This issue can be avoided with a higher flow rate to completely fill the channel, but this will change the shape of the channel, which might not be favorable since squared corners also act as points of stress intensification for the nucleation of cracks. Another possibility is to use a less viscous slurry and/or lower speed of the doctor blade, giving more time to the slurry to flow inside the empty regions of the channel. A third approach could be to change the tool used to machine the channel. If the tool had a round tip (instead of flat), the bottom of the channel would result in a convex shape, which could possibly better fit the round-shape of the channel and of the extrusion tip. Nevertheless, Fig. 5 shows a good bonding between layers, without visible delamination even near the channel.

3.4. Evaluation of the channel connectivity

A direct assessment of the channel continuity is possible after the manufacturing process, already in the green state. As the ink employed in this project is based on graphite, the deposited filament forms an electrically conductive path in an isolating material (the surrounding porcelain). Thus, the two extremities of the channel were connected to a simple electrical circuit and an LED light was used to visualize the continuity of the circuit.

Fig. 6 shows the simple arrangement used for this evaluation. The porcelain plate in the figure contains an embedded channel system, which was designed to have two distinct inlets starting at the side of the part and converging into a single output on the top surface of the ceramic. The dashed line in Fig. 6a is a representation of the design of the channel.

Connecting an LED light and a battery to the part, the channel turns into an electric circuit. When the circuit is closed (Fig. 6b) the LED light switches on. This simple evaluation was performed before any heat treatment and can be used to validate the hybrid manufacturing process. In case of issues in the deposition such as bubbles or misalignment of the extruder, the continuity of the channel can be interrupted, which is easily verified in this setup.

A further evaluation of the channel path and continuity after heat treatment was assessed by micro-computed tomography (μCT). Fig. 7 displays a set of images reconstructed from the μCT scan of a part with a complex design of the channel. Different from the channel design of Fig. 3, this part contains a V-shaped channel which is crossing a straight channel in two points without interception, following a path first above and then below it (in respect to the thickness of the porcelain plate).

Fig. 7b–e shows four regions of interest inside the part with the 3D channel, with respective cross-sections (blue planes). The first region in Fig. 7b shows the two channels at different deposited layers during the manufacturing process. Fig. 7c shows the region with the first crossing of the channels. From this cross-section it is possible to see that, although the channels are very close, there is no connection between them. Fig. 7d shows the second crossing point of the channels, now at inverted layer height. Finally, in Fig. 7e the channels reach their final position, swapping positions in respect to the thickness of the plate compared to Fig. 7b.

A video showing an animation of successive cross-sections of the μCT reconstructed scan can be found in the Supplementary Information (Video 1).

Fig. 8 shows a simple mixer for two fluids following the design shown in Fig. 6, consisting of two input channels embedded in a sintered porcelain plate. The two channels join in the middle, forming a S-shaped channel that end into a vertical output for the mixture of the two fluids. Two syringes with dyed water were used as input liquids (yellow and blue). A third syringe was connected to the output of the channel, where the green water emerged as shown in Fig. 8. In addition, a video of the experiment with this channel setup can be seen in the Supplementary Information (Video 2), which better shows the mixing of the liquids.

Supplementary video related to this article can be found at https

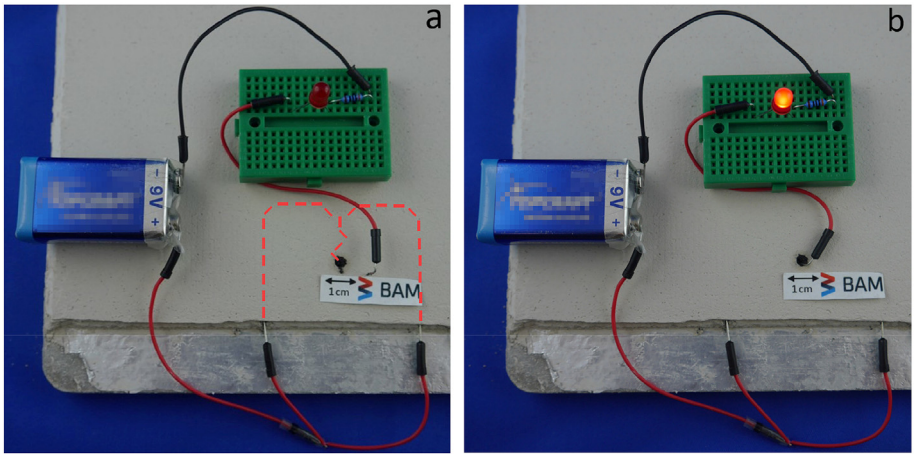

Fig. 6. Test of the connectivity of the channel in the green state. (a) A simple circuit is connected to the electrically conductive graphite ink filling the channel. (b) If the graphite ink is not interrupted by defects, the LED lights up. The dashed red line indicates the shape of the channel inside of the porcelain layers. (For interpretation of the references to colour in this figure legend, the reader is referred to the Web version of this article.)

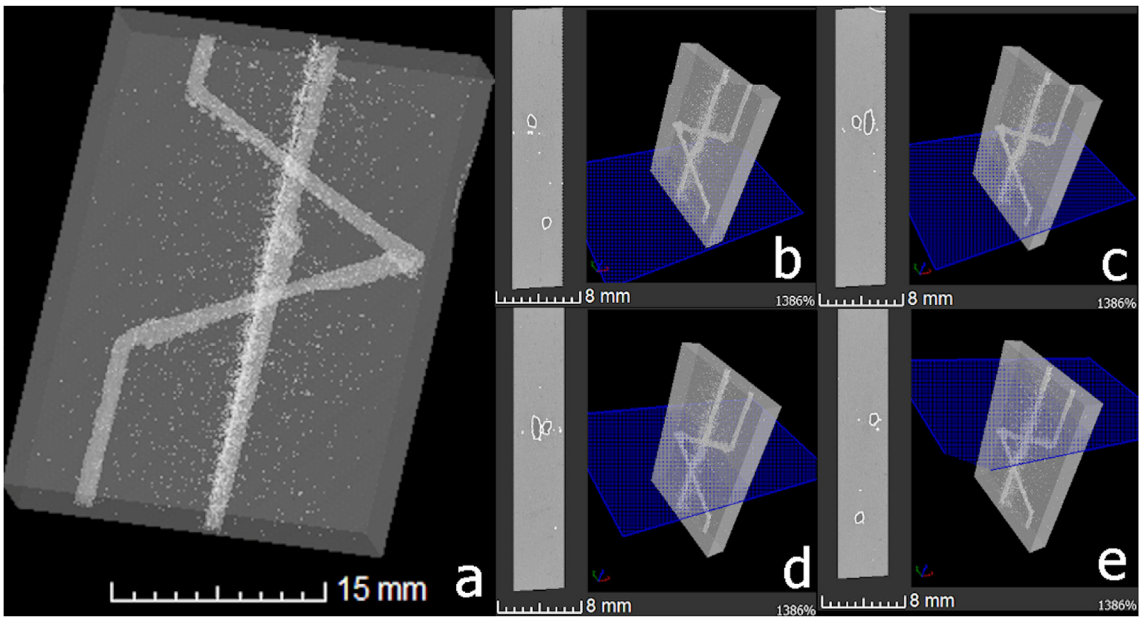

Fig. 7. Reconstruction of a μCT analysis of a porcelain part with embedded 3D channel (a), showing different cross-sections (b–e).

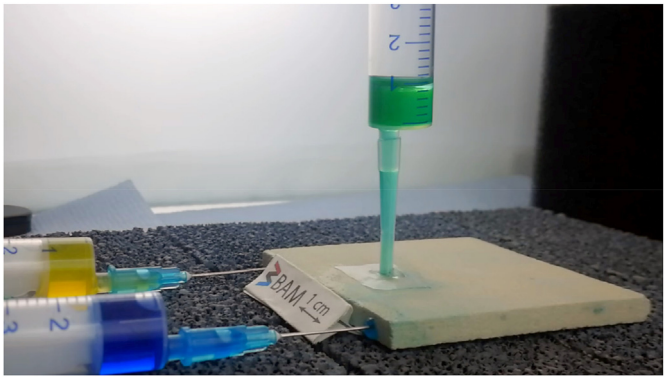

Fig. 8. Demonstration of mixing a yellow and a blue liquid inside of a porcelain sample manufactured by LSD-DIW.

://doi.org/10.1016/j.oceram.2020.100010

4. Conclusions

This work introduces the first results of a new hybridization process that can produce ceramic parts with channels or other complex internal features using a sacrificial graphite-based ink. The ceramic part is fabricated layer-by-layer by the Layerwise Slurry Deposition process combined with end milling and with Direct Ink Writing, enabling the fabrication of dense ceramic parts with inner cavities. Both milling and ink deposition can impact the overall quality of the channels and must be controlled to create a well-shaped channel. Even though the work described in this manuscript is still at the early stages of optimization, it was shown that this process is suitable to produce inner cavities with complex shapes, not only in a single layer but also in a three-dimensional configuration.

5. Outlook

Further development in this project will involve the application of the LSD-DIW hybrid AM technology to the use of a conductive ink, in order to integrate electronic circuits or heating elements in a ceramic insulating substrate. The combination of conductive and insulating elements by multi-material and/or hybrid AM enables the fabrication of multi-functional components in a single process [25–28].

The hybrid LSD-DIW can also be further integrated with other technologies such as binder jetting (BJ), similar to other applications of the LSD [21,29], adding a step to the hybrid process: (i) LSD deposition of ceramic powder layers, (ii) binder jetting to selectively inscribe a cross-section in the layer (iii) milling in the binder jetted area of the layer and (iii) deposition of an ink (ceramic, metallic or polymeric) by direct ink writing (DIW) to fill the machined volume. The LSD-BJ-DIW hybrid process will offer the additional possibility to produce multi-material components with a complex-shaped 3D ceramic phase.

The major benefit envisioned for the LSD-BJ-DIW technology in comparison to extrusion-based multi-material AM approaches (using a second extrusion head to deposit a sacrificial material [1] or additional material phases [25]) is that the ceramic layers deposited by LSD provide a stiff and stable support both to the entire part and to the material deposited by DIW. Multi-material DIW, on the other hand, offers a higher flexibility for alternating two or multiple material phases, while the LSD-DIW is better suited for components with a main ceramic phase in which elements of a secondary phase are embedded.

An approach similar to the one described in this work is the hybridization of ceramic vat photopolymerization and DIW (hybrid VP-DIW). In the hybrid VP-DIW, which was recently proposed [27], a photosensitive resin highly filled with ceramic particles is spread to deposit thin layers, and a second material is introduced in the layers by DIW. While VP-DIW can provide parts with better surface finish due to the high resolution of the VP process, the major benefit of LSD-BJ-DIW is that the ceramic layers deposited by LSD are comparable to ceramic green bodies produced by slip casting or isostatic pressing. Consequently, the machining and the final firing steps in the LSD-BJ-DIW are comparable to the green machining and its related know-how which is available in the ceramic industry. Furthermore, the use of support structures, which is common in VP, is not necessary in the LSD due to the stability of the powder layers.

Declaration of competing interest

The authors declare the following financial interests/personal relationships which may be considered as potential competing interests: G. Franchin and A. Zocca were guest editors for Open Ceramics at the time of the submission. J. Günster was associate editor for Open Ceramics at the time of the submission. According to the journal's policy, the

submission was managed by a different editor.

Acknowledgements

The authors are grateful to the JECS Trust (Contract No. 2018168) and to the BAM Internal Program for guest scientists for funding the visits of Giorgia Franchin to BAM.

Appendix A. Supplementary data

Supplementary data to this article can be found online at https://doi.org/10.1016/j.oceram.2020.100010.

References

[1] C. Xu, B. Quinn, L.L. Lebel, D. Therriault, G. L'espérance, Multi-material direct ink writing (DIW) for complex 3D metallic structures with removable supports, ACS Appl. Mater. Interfaces 11 (8) (27 2 2019) 8499–8506.
[2] A. Bournias-Varotsis, R.J. Friel, R.A. Harris, D.S. Engstrøm, Ultrasonic Additive Manufacturing as a form-then-bond process for embedding electronic circuitry into a metal matrix, J. Manuf. Process. 32 (1 4 2018) 664–675.
[3] D. Zhang, W. Jonhson, T.S. Herng, Y.Q. Ang, L. Yang, S.C. Tan, E. Peng, H. He, J. Ding, A 3D-printing method of fabrication for metals, ceramics, and multi-materials using a universal self-curable technique for robocasting, Mater. Horizons 7 (4) (2020) 1083–1090.
[4] Y. Chivel, New approach to multi-material processing in selective laser melting, Phys. Procedia 83 (2016) 891–898.
[5] J. Koopmann, J. Voigt, T. Niendorf, Additive manufacturing of a steel–ceramic multi-material by selective laser melting, Metall. Mater. Trans. B Process Metall. Mater. Process. Sci. 50 (2) (2019) 1042–1051.
[6] R. Falck, J.F. dos Santos, S.T. Amancio-Filho, Microstructure and mechanical performance of additively manufactured aluminum 2024-t3/acrylonitrile butadiene styrene hybrid joints using an addjoining technique, Materials 12 (6) (2019) 864.
[7] M.P. Sealy, G. Madireddy, R.E. Williams, P. Rao, M. Toursangsaraki, Hybrid processes in additive manufacturing, J. Manuf. Sci. Eng. 140 (6) (2018).
[8] D.S. Choi, S.H. Lee, B.S. Shin, K.H. Whang, Y.A. Song, S.H. Park, H.S. Jee, Development of a direct metal freeform fabrication technique using CO_2 laser welding and milling technology, J. Mater. Process. Technol. 113 (2001) 1273–3279.
[9] Z. Zhu, V.G. Dhokia, A. Nassehi, S.T. Newman, A review of hybrid manufacturing processes–state of the art and future perspectives, Int. J. Comput. Integrated Manuf. 26 (7) (2013) 596–615.
[10] Z. Zhu, V. Dhokia, S.T. Newman, A. Nassehi, Application of a hybrid process for high precision manufacture of difficult to machine prismatic parts, Int. J. Adv. Manuf. Technol. 74 (5–8) (2014) 1115–1132.
[11] J. Li, T. Wasley, T.T. Nguyen, V.D. Ta, J.D. Shephard, J. Stringer, P. Smith, E. Esenturk, C. Connaughton, R. Kay, Hybrid additive manufacturing of 3D electronic systems, J. Micromech. Microeng. 26 (10) (2016) 105005.
[12] A.J. Lopes, E. MacDonald, R.B. Wicker, Integrating stereolithography and direct print technologies for 3D structural electronics fabrication, Rapid Prototyp. J. 18 (2) (2012) 129–143.
[13] D. Espalin, D.W. Muse, E. MacDonald, R.B. Wicker, 3D Printing multifunctionality: structures with electronics, Int. J. Adv. Manuf. Technol. 72 (5–8) (2014) 963–978.
[14] F. Vogeler, W. Verheecke, A. Voet, H. Valkenaers, An initial study into Aerosol Jet® printed interconnections on extrusion based 3D printed substrates, Strojniski Vestnik-J. Mech. Eng. 59 (11) (2013) 689–696.
[15] X. Tian, T. Mühler, C. Gomes, J. Günster, J.G. Heinrich, Feasibility study on rapid prototyping of porcelain products, J. Ceram. Sci. Technol. 2 (4) (2011) 217–225.
[16] T. Mühler, C. Gomes, M.E. Ascheri, D. Nicolaides, J.G. Heinrich, J. Günster, Slurry-based powder beds for the selective laser sintering of silicate ceramics, J. Ceram. Sci. Technol. 6 (2) (2015) 113–118.
[17] U. Scheithauer, E. Schwarzer, T. Moritz, A. Michaelis, Additive manufacturing of ceramic heat exchanger: opportunities and limits of the lithography-based ceramic manufacturing (LCM), J. Mater. Eng. Perform. 27 (1) (2018) 14–20.
[18] D.M. Murphy, A. Manerbino, M. Parker, J. Blasi, R.J. Kee, N.P. Sullivan, Methane steam reforming in a novel ceramic microchannel reactor, Int. J. Hydrogen Energy 38 (21) (2013) 8741–8750.
[19] U. Scheithauer, E. Schwarzer, G. Ganzer, A. Kornig, W. Becker, E. Reichelt, M. Jahn, A. Har-tel, H. Richter, T. Moritz, Micro-Reactors Made by Lithography-Based Ceramic Manufacturing (LCM), vol. 258, Additive Manufacturing and Strategic Technologies in Advanced Ceramics: Ceramic Transactions, 2016, pp. 31–41.
[20] W.H. Herschel, R. Bulkley, Konsistenzmessungen von Gummi-Benzollösungen, Kolliud Zeitschrift 39 (1926) 291–300.
[21] A. Zocca, P. Lima, J. Günster, LSD-based 3D printing of alumina ceramics, J. Ceram. Sci. Technol. 8 (1) (2017) 141–148.
[22] J.E. Smay, J. Cesarano, J.A. Lewis, Colloidal inks for directed assembly of 3-D periodic structures, Langmuir 18 (14) (2002) 5429–5437.
[23] K. Cai, B. Román-Manso, J.E. Smay, J. Zhou, M.I. Osendi, M. Belmonte, P. Miranzo, Geometrically complex silicon carbide structures fabricated by robocasting, J. Am. Ceram. Soc. 95 (8) (2012) 2660–2666.
[24] E. Peng, X. Wei, U. Garbe, D. Yu, B. Edouard, A. Liu, J. Ding, Robocasting of dense yttria-stabilized zirconia structures, J. Mater. Sci. 53 (2018) 247–273.
[25] J. E. Smay, S. S. Nadkarni and J. Xu, "Direct Writing of Dielectric Ceramics and Base Metal Electrodes".
[26] G.L. Goh, S. Agarwala, G.D. Goh, H.K.J. Tan, L. Zhao, T.K. Chuah, W.Y. Yeong, Additively manufactured multi-material free-form structure with printed electronics, Int. J. Adv. Manuf. Technol. 94 (1–4) (2018) 1309–1316.
[27] J. Raynaud, V. Pateloup, M. Bernard, D. Gourdonnaud, D. Passerieux, D. Cros, V. Madrangeas, T. Chartier, Hybridization of additive manufacturing processes to build ceramic/metal parts: example of LTCC, J. Eur. Ceram. Soc. 40 (3) (2020) 759–767.
[28] J. Günster, T. Rabe and A. Roosen, "Method for producing ceramic multilayer circuit carriers using a slip-based additive manufacturing process". WO Patent WO2016193316A1, 08 12 2016.
[29] P. Lima, A. Zocca, W. Acchar, J. Günster, 3D printing of porcelain by layerwise slurry deposition, J. Eur. Ceram. Soc. 38 (9) (2018) 3395–3400.